Computers in Biology and Medicine 104 (2019) 319–328

Contents lists available at ScienceDirect

Computers in Biology and Medicine

journal homepage: www.elsevier.com/locate/compbiomed

Phase singularity point tracking for the identification of typical and atypical flutter patients: A clinical-computational study

A. Liberos[a,b,*], M. Rodrigo[a,b], I. Hernandez-Romero[b,c], A. Quesada[d], F. Fernandez-Aviles[b], F. Atienza[b], A.M. Climent[b,**,1], M.S. Guillem[a,1]

[a] ITACA Institute, Universitat Politècnica de València, Spain
[b] Cardiology Department, Hospital General Universitario Gregorio Marañón, IiSGM, CIBERCV, Spain
[c] Department of Signal Theory and Communications, Rey Juan Carlos University, Spain
[d] Department of Cardiology, Hospital General Universitari de València, Spain

ARTICLE INFO

Keywords:
Atrial flutter
Phase map
Cardiac model
Body surface potential mapping

ABSTRACT

Atrial Flutter (AFL) termination by ablating the path responsible for the arrhythmia maintenance is an extended practice. However, the difficulty associated with the identification of the circuit in the case of atypical AFL motivates the development of diagnostic techniques. We propose body surface phase map analysis as a non-invasive tool to identify AFL circuits.

Sixty seven lead body surface recordings were acquired in 9 patients during AFL (i.e. 3 typical, 6 atypical). Computed body surface phase maps from simulations of 5 reentrant behaviors in a realistic atrial structure were also used. Surface representation of the macro-reentrant activity was analyzed by tracking the singularity points (SPs) in surface phase maps obtained from band-pass filtered body surface potential maps.

Spatial distribution of SPs showed significant differences between typical and atypical AFL. Whereas for typical AFL patients 70.78 $\pm$ 16.17% of the maps presented two SPs simultaneously in the areas defined around the midaxialliary lines, this condition was only satisfied in 5.15 $\pm$ 10.99% ($p < 0.05$) maps corresponding to atypical AFL patients. Simulations confirmed these results.

Surface phase maps highlights the reentrant mechanism maintaining the arrhythmia and appear as a promising tool for the noninvasive characterization of the circuit maintaining AFL. The potential of the technique as a diagnosis tool needs to be evaluated in larger populations and, if it is confirmed, may help in planning ablation procedures.

1. Introduction

Atrial flutter (AFL) is defined as an atrial macro-reentrant tachycardia maintained by an electrical wavefront rotating continuously around an anatomical structure, a scar or a functional block area. AFL is manifested in the electrocardiogram (ECG) by repeating atrial complexes with a constant morphology at a rate of 250–300 beats per minute [1]. Depending on the structure that defines the reentrant circuit, AFL is subdivided into two categories: typical AFL, caused by a rotation around the tricuspid annulus (TA) and atypical AFL, caused by a rotation around any other structure either in the left or right atria [2]. AFL can be terminated by ablation of some segment of the reentrant circuit, preferentially the narrowest portion of the circuit [3]. While in typical AFL ablation of the cavotricuspid isthmus consistently results in an effective arrhythmia termination [1,4], identification of the ablation target in atypical AFL requires extensive invasive mapping studies in order to determine the circuit responsible of the arrhythmia, which may be especially complex in case of AFL secondary to prior surgical procedures [5].

In addition, current noninvasive classifications of regular atrial tachycardias and atrial flutter have been based exclusively on the standard ECG properties. The classification is mainly based on a rate cut off and the presence or absence of isoelectric baselines between atrial deflections [2,3]. However, the understanding of the mechanisms that

* Corresponding author. Universitat Politècnica de València, ITACA Institute, ed 8G, accès B, Camí de Vera s/n, 46022, València, Spain.
** Corresponding author. Department of Cardiology, IiSGM Hospital General Universitario Gregorio Marañón, Edificio Materno Infantil C\O'Donnell 48, planta -1, 28009, Madrid, Spain.
E-mail addresses: allimas@itaca.upv.es (A. Liberos), andreu.climent@gmail.com (A.M. Climent).
[1] Drs Guillem and Climent contributed equally to this work and shared senior authorship.

https://doi.org/10.1016/j.compbiomed.2018.11.020
Received 30 April 2018; Received in revised form 24 November 2018; Accepted 26 November 2018

maintain these arrhythmias made this classification inadequate. As a consequence, the characterization of the reentrant circuit is performed invasively during the electrophysiological study that precedes catheter treatment [1]. Noninvasive AFL characterization may increase efficacy and reduce duration of catheter ablation procedures.

Phase map analysis has been broadly evaluated in the characterization of atrial fibrillation propagation patterns. This signal processing technique helps in the characterization of reentrant patterns and specifically, highlights de axis of rotation, which in atrial fibrillation is associated with the rotors maintaining the arrhythmia. Phase mapping has been used in in-silico [6–8], optical mapping [9] and body surface map [10] atrial fibrillation studies.

In this proof–of–concept study, we propose that phase mapping applied to the surface ECG activity will highlight the reentrant activity in AFL patients. That surface phase maps may be dependent on the circuit involved in the reentry and thus, may help in the identification of the circuit maintaining the arrhythmia. With this objective, we analyzed body surface phase maps of AFL patients with either typical or atypical AFL. According with our results, we propose the spatial inscription of phase singularities as a potential tool for identifying the reentrant circuit in AFL patients. The technique was verified by means of computational models and is proposed to be evaluated clinically to assess it as a potential diagnosis tool.

2. Methods

2.1. Patients and body surface potential recording

The study included nine patients admitted at Hospital General Universitario de Valencia with either typical or atypical AFL for an ablation procedure. All patients gave informed consent. The protocol was approved by the Institutional Ethics Committee of the institution.

Recordings were acquired prior to the ablation procedure for 10 min with patients in a supine position. In patients with a heart rate faster than 90 beats per minute, a carotid sinus massage was performed during the recording by a trained physicist in to reduce heart rate and allow a clear recording of AFL waves. A total of 67 electrocardiogram (ECG) signals were obtained covering the entire torso surface (Fig. 1a.), 64 electrodes were arranged in a vest with 36 electrodes in the anterior torso and 28 in the posterior torso plus the limb electrodes [11,12]. Signals were recorded at a sampling rate of 2048 Hz, with a bandwidth of 500 Hz and a resolution of 1 μV. Quality of all leads was visually evaluated before acquisition and stored for off–line processing.

The diagnostic of typical AFL was confirmed in 3 patients in the electrophysiology laboratory by termination of the arrhythmia after cavotricuspid isthmus ablation. The remaining 6 patients had reentrancy circuits not involving the cavotricuspid isthmus and AFL was terminated by electrical cardioversion. (See supplementary material for more details).

2.2. Computational models

2.2.1. Atrial transmembrane potential calculation

Atrial activity was simulated in a volumetric three dimensional model of the human atria consisting in 284,578 vertices and based on the free distribution model developed by Krueger et al. [13]. It includes fiber direction and distinguishes the most important geometric structures allowing customization in terms of propagation. The action potential for each node was mathematically calculated based on the cellular model of human atria proposed by Koivumaki [14].

Remodeling is usually associated with a shortening of the action potentials and reduced diffusion in the cardiac tissue, these properties are present in atrial fibrillation and AFL substrates and facilitate the maintenance of reentrant behaviors [14,15]. We implemented remodeling by increasing gK1 in 31% and decreasing gto, gkur and gCaL in 31%, 19% and 29% respectively, and by decreasing the diffusion (D) in 25%. It represents a remodeling degree in between sinus rhythm conditions and the atrial fibrillation remodeling implemented by Koivumaki et al. [14]. For simulating counterclockwise and clockwise typical AFL, reentrant spread around tricuspid valve was forced; an additional reduction of 40% in D was implemented in cavotricuspid isthmus to account for the reduced conduction velocity that was consistently found in patients [16,17]. (Atypical AFL models in supplementary material).

To help interpretation of surface potentials on the torso surface, we also used a simple model consisting of two concentric spheres as atria and torso. The active tissue of the atria consisted of a 2.5 cm radius sphere incorporating 163,842 nodes (average inter–nodal distance of 236,07 ± 15.35 μm) with two inactive caps. A linear stimulus was applied to induce a rotation around the caps.

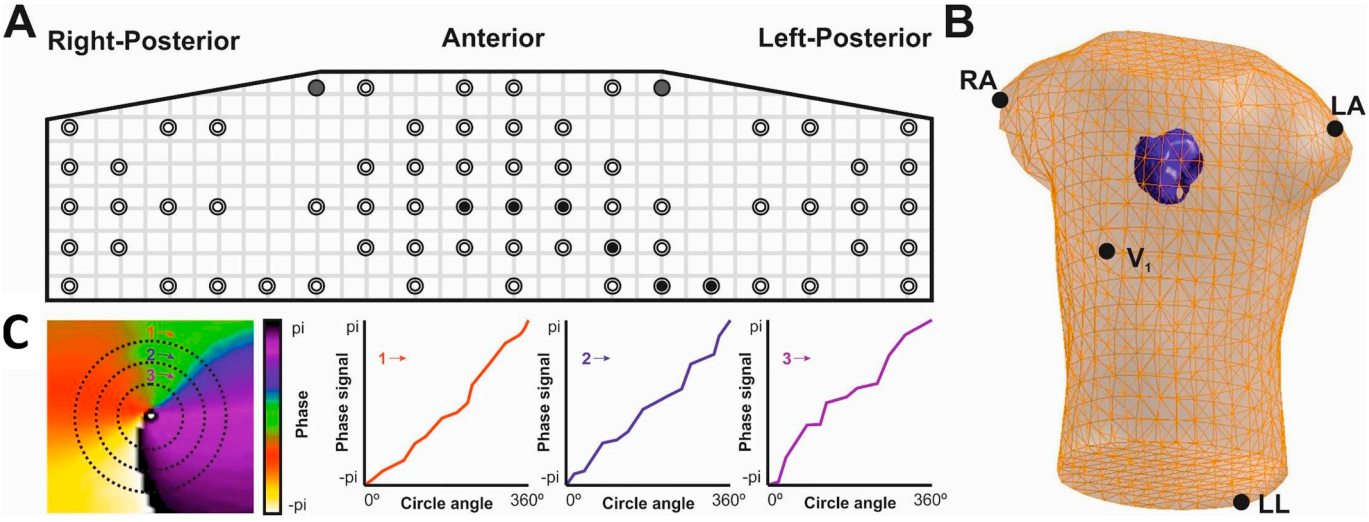

Fig. 1. a) Electrode arrangement in our vest. Light–gray dots show positioning of right and left arm electrodes. Black dots indicate the location of precordial leads (V1–V6). The center of the sketch corresponds with the anterior chest while the left and right parts of the back are represented on the right and left of the figure respectively. b) Atria and torso models. Atrial model with 284.578 nodes is depicted in blue and the torso model with 771 nodes in orange. Nodes corresponding with electrodes: right arm (RA), left arm (LA), left leg (LL) and V1 are depicted as black dots in the figure. c) Phase singularity point (SP) detection methodology. Phase signals are evaluated in three concentric circles around each candidate to be SP. Only those points in which the phase was gradually and monotonically increasing or decreasing in at least two of the three circles are chosen as SP.

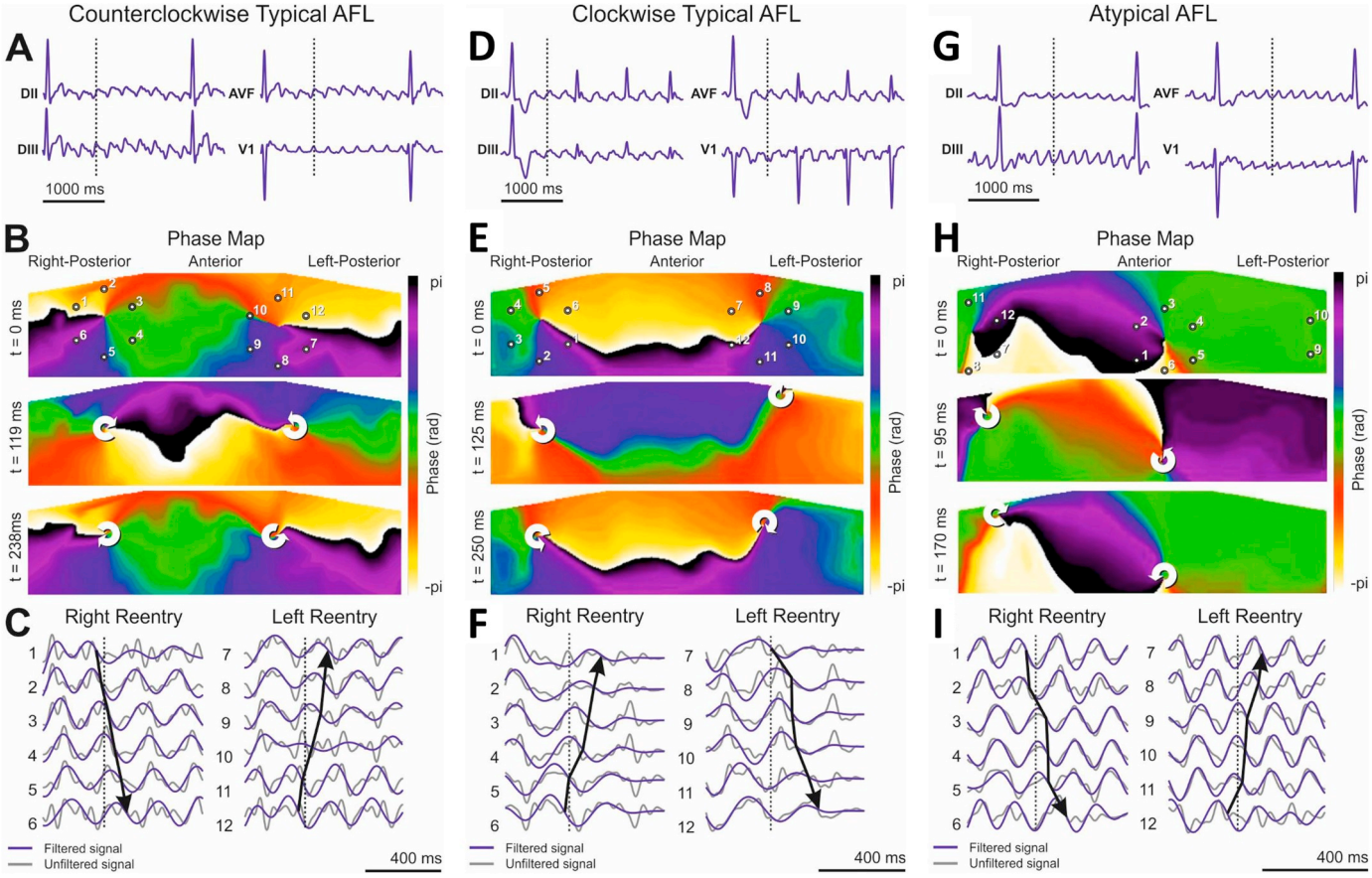

Fig. 2. a, d, g) Inferior ECG leads and V1. b, e, h) Surface phase maps at three consecutive time instants according with Fig. 1a c, f, i) Filtered and unfiltered ECG tracings around phase singularities (for locations represented above) are depicted. Doted vertical lines denote the time instant corresponding to the first surface phase map (t = 0 ms). Points of maximum descending slope of the band–pass filtered signals were connected to highlight the reentrant propagation in the torso.

Numerically the system of differential equations was solved by using the Forward-Euler Rush-Larsen method with time step 5 μs. The calculations were performed on a simulation platform based on a graphic processor unit (NVIDIA Tesla C2075 6G) [18].

2.2.2. Torso potential calculation

Simulated electrograms (EGMs) in 2048 points distributed around the epicardium were calculated by using the transmembrane potentials calculated in simulations. Torso potentials were obtained by calculating the forward problem of electrocardiography by applying the Boundary Element Method [10,19,20]. Specifically, ECGs were computed on a torso model with 771 nodes and 1538 faces [21] in the case of the realistic model (Fig. 1b.), and a sphere of 2562 nodes and 5120 faces in the case of the spherical model. Homogeneous and isotropic conductivities assigned to each conductor volume were 0.3 S/m in the case of blood –inside the atria– and 0.2 S/m for the rest of torso tissues.

2.3. Signal processing

Patient signals were preprocessed as previously described [12]. Briefly, baseline oscillations were reduced by subtracting the estimated baseline. To estimate the baseline, ECG signals were decimated to 51.2 Hz and filtered with a Butterworth 10th-order low-pass filter with a cut-off frequency of 2 Hz. Baseline was then interpolated to 2048 Hz and subtracted to the original signal. Segments free from ventricular content longer than 400 ms were selected after automatic detection of fiducial points of QRSonset and T–waveoffset. The five longest segments free from ventricular content for each patient were included in the study. In the case of computational models, we used the ECG signals obtained with the forward problem of electrocardiography.

The resulting ECG signals were filtered, by means of a 4 Hz bandwidth band–pass filter, around the reentrant frequency. In the case of models, the reentrant frequency is easily measurable; the most predominant dominant frequency found on the torso surface was used for patients. To do so, the dominant frequency in each lead was computed by using the Fast Fourier transform with a resolution of 0.5 Hz. Body surface potential maps were obtained from the filtered ECG signals by cubic spline interpolation.

2.4. Phase maps and phase singularity point tracking

Body surface phase maps were obtained from potential maps by calculating the instantaneous phase for each point by using the Hilbert transform [6,8,10]. The phase signal ranges from -pi to pi and represents the relative delay of each signal in one period. A phase singularity point (SP) is defined as the point in a phase map which is surrounded by phases from –pi to pi.

To increase reliability, the phase values were obtained along 3 different circles surrounding each evaluated point with radii 0.06, 0.12 and 0.2 the height of the torso. An evaluated point was defined as a SP only when the phases of at least two of these three circles were gradually and monotonically increasing or decreasing for a total of 2π (Fig. 1c.). SPs were tracked in time and space and only SPs lasting for at least half rotation were considered. Spatial occurrence of SPs was quantified into histograms, two-dimensional recurrence maps were represented for patients, histograms were represented directly on the torso surface for computational models.

2.5. Statistical analysis

Student's T–test was used to evaluate the statistical significance between continuous unpaired variables, and statistical significance was considered for $p < 0.05$. All data are reported as mean ± SD (standard deviation).

3. Results

3.1. Surface phase maps of typical and atypical atrial flutter patients

Stable rotational patterns can be observed in consecutive surface phase maps of typical AFL patients (Fig. 2). Surface phase maps of typical counterclockwise AFL patients (Panel B) display a craniocaudal propagation pattern on the anterior torso and the opposed direction on the posterior torso. Two SPs appear on both midaxillary lines at the center of each rotational pattern and remain stable for consecutive propagations. This propagation was consistent with a counterclockwise rotation around the tricuspid valve with a descending propagation in the right atria free wall followed by an ascending propagation in the interatrial septum.

Fig. 2a shows standard leads with a morphology coherent with previous studies [1,17] with biphasic and positive deflections on lead V1 and a complex undulation in inferior leads described as a slow descending phase followed by a pronounced negative slope; and finally an ascending slope that ends with a positive deflection that connects with the following wave.

Fig. 2c shows how band–pass filtered ECG signals highlights the reentrant behavior, but this rotational pattern becomes more evident in the surface phase maps.

In a case of clockwise typical AFL, surface phase maps display a caudocranial propagation pattern on the anterior torso followed by propagation in the opposite direction in the back, consistent with a clockwise rotation around the tricuspid valve (Fig. 2e.). Again, two SPs appear on both midaxillary lines and, as for the counterclockwise AFL patients, Fig. 2f confirms again the propagation pattern observed in surface phase maps.

The leads shown in Fig. 2d are consistent with those observed in previous studies of typical AFL with a wide, negative and W shape V1 [1]. In the case of inferior leads complex tracings similar to those observed in counterclockwise typical AFL without silence periods because of the constant reentry can be observed.

An example of an atypical AFL patient is presented in Fig. 2g–i. In this case, the standard ECG does not allow identifying the circuit involved in the reentry (Fig. 2g.) as it does not present a recognizable pattern, positive deflections can be observed in the inferior leads and biphasic waves in V1, continuous waves with short silent periods can be observed in accordance with a constant reentry in the atria.

Surface phase maps show again two SPs, but in this case the locations differ from those observed in the case of typical AFL patients. In this case, SPs are located in the anterior and right–posterior part of the torso, showing a counterclockwise propagation in the front.

Fig. 3a shows occurrence maps for SPs of both typical and atypical AFL patients. SPs of typical AFL patients are presented in the top panel, these SPs are clustered in the same region (midaxillary lines, displayed as shaded areas on the surface maps) regardless of the rotation direction. P1 (patient 1) corresponds with the CCW AFL patient presented in Fig. 2a–c and P2 corresponds with the example of CW AFL patient presented in Fig. 2d–f.

SPs of atypical AFL patients do not consistently match with the typical AFL SP locations. P9 in Fig. 3a corresponds with the example shown in Fig. 2g–i. As presented before, the presence of SPs is more predominant in the anterior and right–posterior part of the torso. P4 and P5 show a distribution of SPs similar to the observed in P9 anterior and right–posterior part of the torso but with different latitudes. Finally, P6, P7 and P8 presented a scattered distribution on the torso.

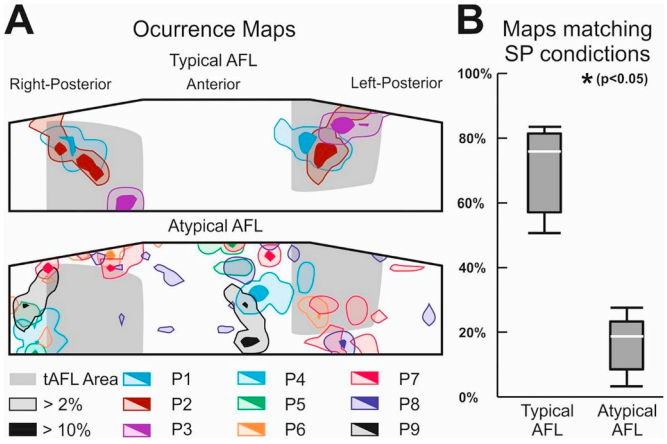

Fig. 3. a) Anatomical regions at which SPs were detected during more than the 10% (solid colors) and 2% (shaded colors) of the analyzed maps are depicted. The gray shading represents the typical AFL area, right and left areas were used to evaluate if the maps contained two simultaneous SPs in these regions. b) Box plot representing the percentage of maps that accomplished SP conditions for both typical and atypical AFL patients. Significant differences can be observed between both groups.

Note that in all cases the SPs are clustered in contralateral views of the torso, which is consistent with the figure–of–eight patterns shown in surface phase maps.

By defining the shaded area in Fig. 3A as the typical AFL SP area, we evaluated the number of maps for each patient that presented simultaneously a SP in each of the two defined typical AFL SP areas. In the case of typical AFL patients 70.78 ± 16.17% of their maps accomplished the conditions described. Oppositely, 5.15 ± 10.99% ($p < 0.05$) of maps matched these conditions for atypical AFL patients (Fig. 3b).

3.2. Understanding torso surface phase maps

Notice that surface phase maps of AFL patients display figure–of–eight patterns. In Fig. 4a–c, computer simulations of a rotational pattern in a spherical model show that this figure–of–eight pattern appears as the projection of a single rotation on two contralateral views and does neither imply a dual–loop reentry nor the existence of functional rotors. SPs on the surface arise in the intersection of the axis of rotation of the propagation with the surface of the torso and thus appear at the same location for a given propagation circuit regardless of the rotation direction.

The spherical model has the advantage that, because of the geometrical simplicity the propagation in the torso, the relation between reentrant patterns between the inter and outer layers is easily understood. However, in the case of realistic geometries, the contribution of wave fronts propagating in different planes makes harder the estimation of torso propagation. With this aim we evaluated the location of SP from atria to torso by using a multilayer (N = 9) model.

Fig. 4d shows the evolution of SPs from the atria to the torso in the case of a typical AFL (Fig. 5). We define filament as the connection between SPs in the different layers (see supplementary material) [10]. It can be observed how in the most internal layer SPs are closer to the center of the reentrant circuit, and how the filament is slightly deflected according to the weight of the electrical activity observed in the realistic model. It means that, as the descending propagation corresponds only to that observed in the right atria free wall and the ascending propagation both to the septum and left atria this imbalance of electric charge results in a deflection of the filament to the anterior part of the torso. This explains the placing of SPs depending on the reentrant circuit in the atria. The SPs in the outer layer occupy positions close to that previously observed in patients.

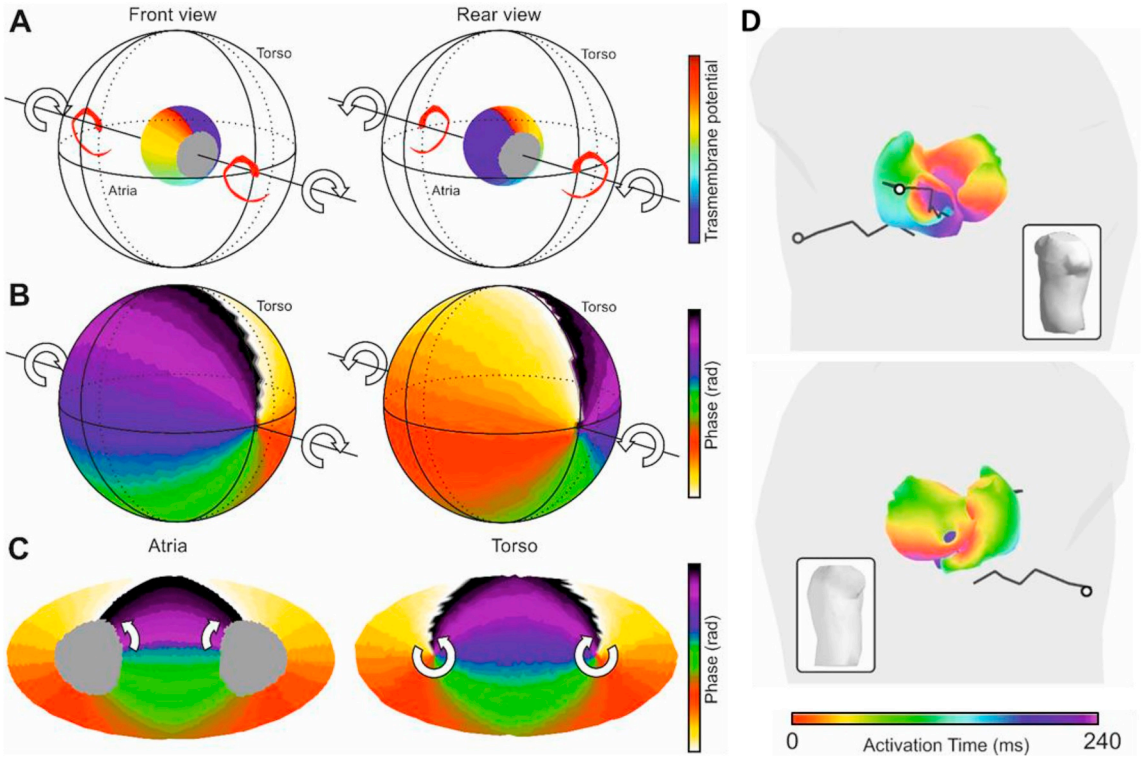

Fig. 4. a) Two opposing viewpoints of a simulated activity in a model that includes atrial tissue, torso volume and torso surface. Atrial voltage maps are represented according to a color scale from blue to red. The simulated activity consists of a stable reentry around an anatomical obstacle. b) Propagation of electrical activity on the outer sphere results into a rotational pattern in the phase maps with SPs at the rotation axis. c) Representation into an unfold sphere of the torso electrical activity appears as a figure–of–eight reentry. d) Atria and torso, from two different angles, in a simulation of typical AFL, the top panel shows a view from the left–anterior part of the torso and the bottom panel corresponds to a view from the left posterior part of the torso. Activation time of each part of the atria is presented in the model, a counterclockwise propagation around the tricuspid valve can be observed. SPs obtained in the nine layers covering the volume from the atria to the torso (see supplementary material) are connected with a black line, finally SPs in the torso are highlighted with a white dot.

3.3. Surface representation of simulated atrial flutter episodes

To validate the results, in silico models were used to calculate surface phase maps in different episodes of macro-reentrant tachycardias (i.e. typical and atypical flutters). With the atria and torso models depicted in Fig. 1b and the methods described, it was possible to obtain surface phase maps and the standard leads for each case.

Fig. 5a–c shows, a simulation of counterclockwise typical AFL, in which a reentry around the tricuspid valve can be observed. In the right atrial septum, the propagation has an upward direction, and then a downward propagation was observed in the right atrial free wall. Finally, the circuit crosses the tricuspid annulus and the inferior vena cava to restart the circuit. The whole reentry around this circuit has a period of 242 ms. On the other hand, in the left atrium, it is observed an upward propagation from the base to the pulmonary veins, that takes 175 ms. Both the highest (ms 130) and lowest (ms 195) part of both atria are reached at the same time.

Looking at surface phase maps (Fig. 5b.) we can observe three surface phase maps in three instants of the same period. A downward propagation in the front part of the torso followed by an ascending propagation in the back can be observed, as depicted in three sequential maps. Two SPs are fixed in the midaxillary lines, which is in accordance with the results observed in patients. Note that in silico surface phase maps show the whole torso from clavicles to the top of the pelvic region, while patient register only takes the rib cage.

With respect to standard leads, biphasic and positive deflections in V1, signal representative of counterclockwise typical AFL can be observed. Besides, the complex undulation in inferior leads previously described is also obtained. In the case of DIII a fractionated signal can be observed due to the proximity between the recording point and a SP. The period of the signals corresponds to that observed in the reentry circuit, 242 ms.

According with previous works [17], the ascending slope in AFL tracings corresponds with the depolarization of the upper part of the right atrial free wall, and the positive deflection with the lower part of the wall, the slow descending slope corresponds to the slow propagation across the cavotricuspid isthmus, finally the more pronounced descending slope corresponds to the propagation in the interatrial septum. The positive deflection in V1 corresponds to the wave propagation in the right atrial free wall.

Isocronal maps in Fig. 5d depict a clockwise reentrant activity around the tricuspid valve. An ascending propagation in the right atrial free wall can be observed, after 68 ms the propagation reached the septum and started a descending propagation. Then, the reentrant circuit crossed the area which includes the inferior vena cava and the tricuspid annulus to restart the following period after 242 ms.

With respect to the left atria, the propagation got the structure through the at ms 80. The whole left atrium was depolarized in millisecond 227, being the area between the mitral valve and the left pulmonary veins the last to be depolarized.

Regarding surface phase maps, three different maps corresponding to three time instants in a single period can be observed in Fig. 5e. Two SPs remain in the midaxilliary lines surrounded by a caudocranial propagation pattern on the anterior part of the torso and the opposed direction on the back.

DII and AVF presented important fractionation due to the proximity between an SP and the right arm ECG lead. In the case of DIII, the shape of the waveform is similar to that described for counterclockwise typical flutter and according to that observed in patients. In parallel, V1 shows the negative waves with the W shape characteristic of

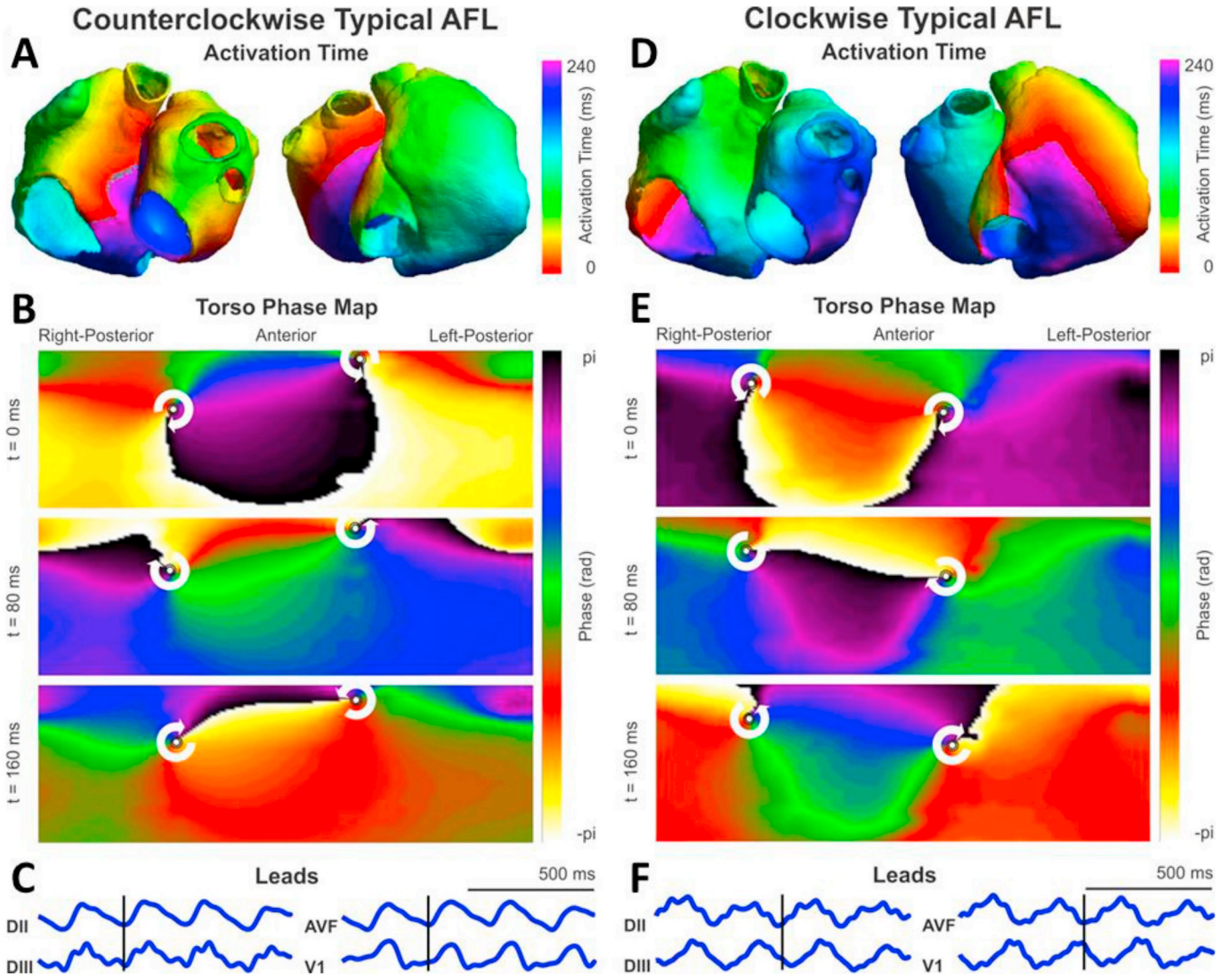

Fig. 5. a, d) Isochronal maps in the atria illustrating typical flutter macro-reentrant behaviors. b, e) Surface phase maps at three consecutive time instants. c, f) Most representative standard derivations in AFL. (See videos in supplementary material).

counterclockwise AFL at the bottom of the signal. This W shape corresponds with the propagation through the right atrial free wall.

Fig. 6a shows the activation times for a macro–reentry with period 240 ms around the 4 pulmonary veins with a functional block region. It can be observed how the front invades the right atrium through the Bachmann's bundle. The right atrium completes its depolarization with an irregular front around crista terminalis.

Surface phase maps depicted in Fig. 6b show a counterclockwise reentrant activity in the upper portion of the posterior torso and a clockwise activity in the anterior torso, showing two SPs in these locations. Note that the upper part of the back is the closest to the pulmonary veins area.

With regard to standard leads, we can see that the inferior leads show no recognizable patterns but allow determining the reentrant rate, however minor alterations due to the low frequency activity promoted in the functional block area are also present. V1 has an important fractionation as it is near the area of the SP. One more example of a reentry around the pulmonary veins can be found in supplementary material.

A simulation of a clockwise reentrant behavior around the inferior vena cava with a period of 269 ms is depicted in Fig. 6d. In the case of the left atrium, the area between the left pulmonary veins and the mitral valve is the last to be depolarized. Phase maps (Fig. 6e) show a SP on the top of the right posterior part of the torso with a counterclockwise activity around it, the second SP is not visible as it corresponds to the base of the torso. It is also observed that there is a sink in the propagation of phase on the upper part of the posterior torso. Regarding the standard leads (Fig. 6f), DII and AVF show fractionation due to the close distance between the right arm electrode and the SP. The period of the tracings is 270 ms, which matches with the rotational period.

Fig. 7 shows the areas of the torso where a SP can be detected for more than 10% of the surface phase maps in each case. Typical AFL SP areas are depicted by the shaded areas in gray. As in the case of patients, the percentage of surface phase maps with points contained simultaneously in both areas has been evaluated. In the case of the counterclockwise and clockwise typical AFL, 100% and 69.87% of maps respectively satisfied the condition. In contrast, only 2.12% of maps satisfied this condition for the reentry around inferior vena cava and 0% and 6.98% in the big and small circuits around pulmonary veins. It reflects a significant difference using this criteria ($p < 0.01$).

Finally, we evaluated the robustness of the method against noise and body size. Fig. 8 shows how the number of maps that match with typical AFL conditions decreases with noise. Note that the noise added to the signal consisted on a randomly generated signal with an amplitude adjusted with the Signal to Noise Ratio (SNR) when compared with

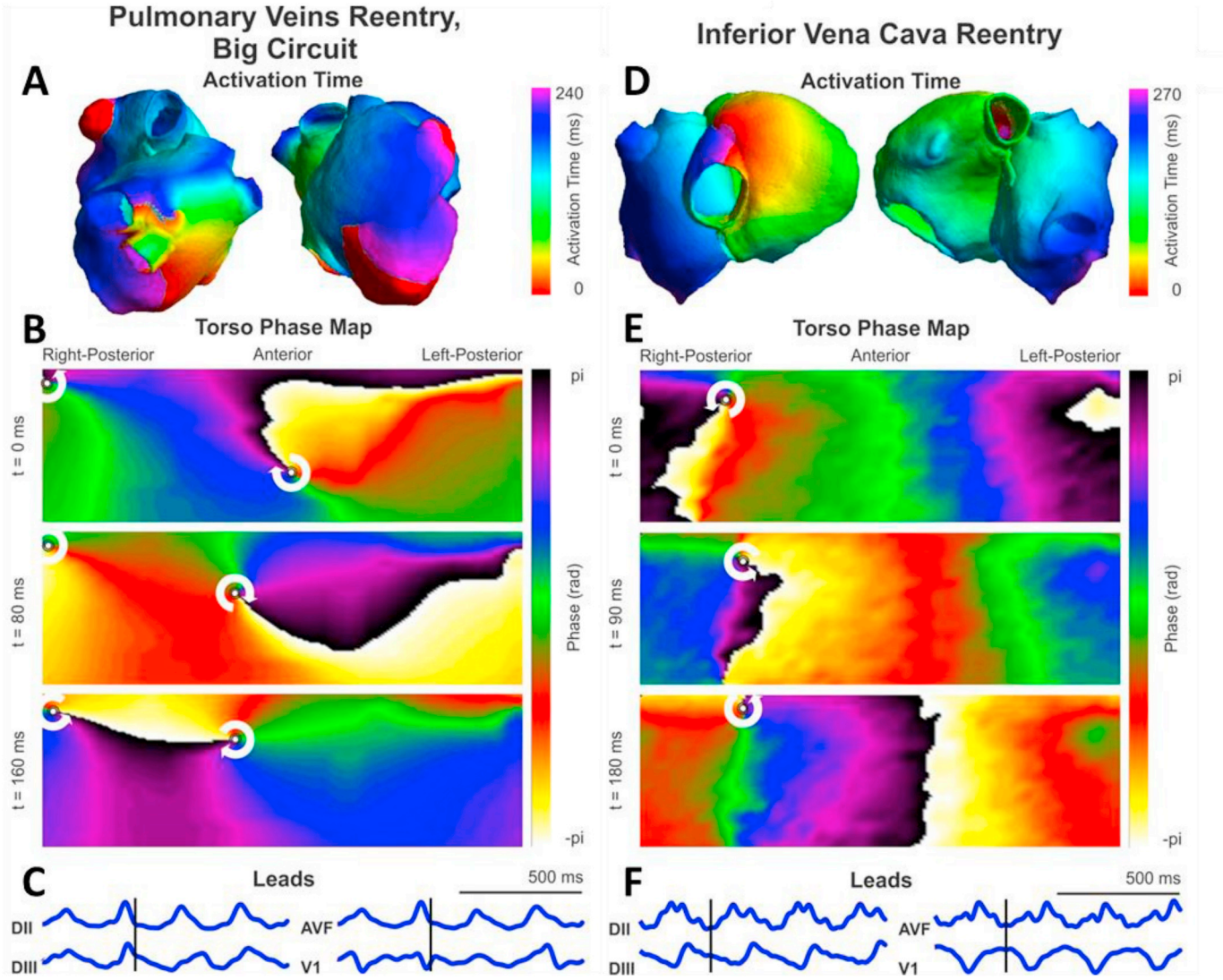

Fig. 6. a, d) Isochronal maps in the atria illustrating macro-reentrant behaviors. b, e) Surface phase maps at three consecutive time instants. c, f) Most representative standard derivations in AFL (one more example in supplementary material).

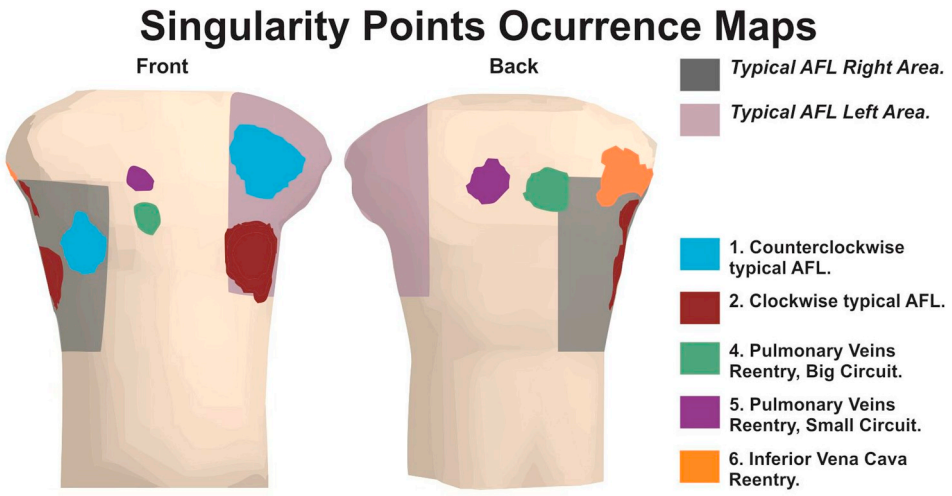

Fig. 7. The regions that show an occurrence of SPs higher than a 10% are depicted for each simulation. Gray shadings represent the typical AFL regions, right and left areas were used again to evaluate if the maps contained simultaneously a SP in each area.

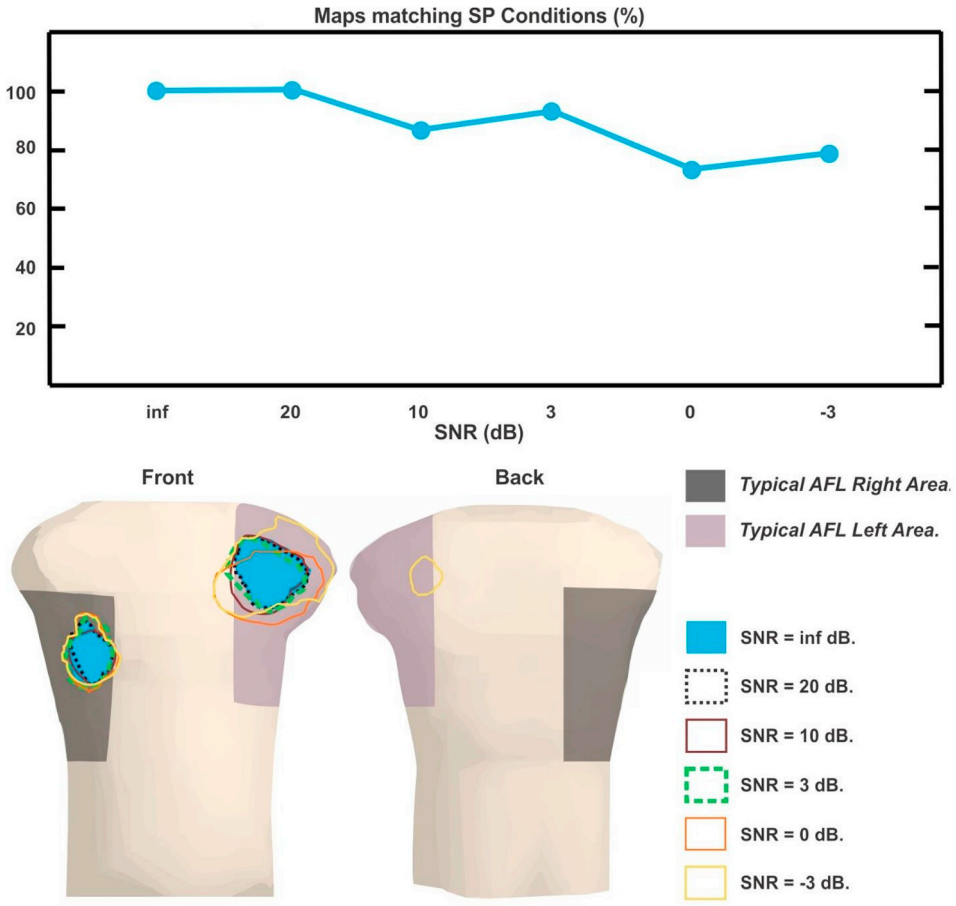

Fig. 8. A decreasing number of maps match with typical AFL conditions with noise. The regions that show an occurrence of SPs higher than a 10% are depicted for each level of noise in the counterclockwise typical AFL simulation.

the ECG signal with the maximum amplitude. Despite the amount of noise added, which may affect dramatically an activation detection-based analysis technique, SP locations are quite robust thanks to the methodology presented.

We evaluated the technology in terms of sensitivity to the size of the torso with two bigger models (waist measurement 135 and 115 vs. 100 cm). Thinking in a homogeneous distribution of electrodes, typical AFL areas were defined according the new body sizes. 100% of the maps accomplished the condition for the model with the size closer to the original one and 90.70% for the biggest one (see Fig. S3 in supplementary material).

3.4. Detection of the reentrant frequency from the torso

Computer models were used to assess the ability to detect the rotation period of reentries in AFL from the torso surface. We used the Fast Fourier transform to detect, both in the computed ECGs and EGMs, the dominant frequency with resolution 0.5 Hz. In the case of typical AFL, the reentries around the inferior vena cava and the big circuit around pulmonary veins 90.89 ± 9.31% ECG signals presented as dominant frequency the observed in the reentry. Moreover, in the EGMs, the frequency of reentry was detected in 90.54 ± 11.12% nodes. The case of the small reentrant circuit in pulmonary veins presented the frequency of the reentry in the 56.87% of the EGs and in the 58.97% of the ECGs. This shows the ability to estimate the dominant frequency of the reentry from the ECG leads in the case of AFL.

4. Discussion

4.1. Major findings

In this study, body surface phase mapping is proposed as a non-invasive technique to distinguish between cavotricuspidius dependent and non–dependent atrial macro-reentries. We show that surface phase maps obtained from body surface potential recordings from patients with AFL display characteristic figure–of–eight patterns that arise as a projection of a single rotation into two contralateral views. SPs location on surface phase maps is determined by the intersection of the rotation axis with the surface of the torso, and thus is distinct depending on the rotation circuit. This may help in a noninvasive determination of the rotation circuit in complex atypical AFL.

The technique has been evaluated both in patient recordings and by using computational modeling. For typical AFL patients we observed that SPs were in limited regions around the axillary lines. However, in the case of patients of atypical AFL the location of SPs was not restricted to these areas. The same applies in the case of computer modeling simulations, where we verified that the location of the SPs depends on reentrant circuit. It can be observed that in these cases the points may be associated with a projection of the obstacle on the surface of the torso, although some deviation is produced by the propagation through the rest of the atria, as depicted in Fig. 4.

To stabilize the reentrant spread on the torso surface and help visualize the points, the signals at the torso were band–pass filtered with a bandwidth of 4 Hz around the frequency of reentry. In the case of

patient recordings, this frequency was estimated as the most repeated dominant frequency between all electrodes. It is consistent with the analysis of dominant frequencies in models presented and with previous work presented by the group where band–pass filtering was used to noninvasively characterize dominant reentrant sources during atrial fibrillation [8,10].

4.2. Noninvasive diagnosis of atrial flutter from the surface ECG

The surface ECG is routinely used for establishing the diagnosis of AFL because of its characteristic undulating pattern. The ECG can also be used for a first identification of the circuit involved in the reentry [22]. A sawtooth pattern in the inferior ECG leads is suggestive of a cavotricuspidius dependent AFL. However, age–related fibrosis, pulmonary disease and prior surgery can alter the surface ECG signals [2,23,24] and 13% of patients with cavotricuspidius dependent circuits had neither sawtooth waves nor RR regularity [25]. According to that presented in the noise analysis in Fig. 8, our presented surface phase maps may be less sensitive to these alterations since subtle changes in propagation will not alter the overall rotational pattern.

Less commonly, the reentrant circuit involves anatomical locations different that the cavotriscuspid isthmus. In these cases, classified as atypical atrial flutter, analysis of atrial waves on the standard ECG does not report feasible information about the reentrant circuit since there is high variability either in terms of shape, base line or frequency [1,26]. Differentiation between left and right AFL has motivated many previous works. Left atrium AFL has been shown to present shorter cycle lengths than isthmus dependent AFL in post–radiofrequency MAZE patients [24] and lower spatial coherence [27], which is consistent with the scattered SP histograms corresponding to some AFL patients. These limitations resulted in localization of the reentry based mainly in invasive electrophysiology mapping studies prior to catheter ablation.

Current differentiation of regular atrial tachycardias and atrial flutter patients is also based on standard ECG analysis. The differentiation is based on a rate cut off and the presence or absence of isoelectric baselines between atrial deflections [2,3]. However, this classification may be not robust enough according with the different mechanisms that maintain the arrhythmia and it is critical when choosing antiarrhythmic or ablation treatments. As an alternative approach to the standard ECG, Sippensgroenewegen et al. [16] proposed the use of integral maps obtained from body surface potential recordings to identify patients with typical AFL. However, it has not been shown that integral maps of atypical AFL patients allow discrimination from typical AFL patients.

In this proof-of-concept study, we have shown that the rotational patterns depicted in surface phase maps of AFL patients highlight the reentrant mechanism maintaining the arrhythmia. That surface phase maps of atypical AFL patients differ from those of typical AFL patients because of their different rotation axes. Clustered SP occurrence maps are observed in typical and most atypical AFL patients according with the consistency and repeatability of the reentrant patterns. Scattered SP occurrence maps may prevent the clinicians for low spatial consistency of the arrhythmia, and thus, a more complex procedure. This new technique, should help for guidance of the clinical cardiologist and electrophysiologists, providing information about their anatomic substrates and improving treatment strategies selection. Nevertheless, its potential as a new diagnosis tool will need to be tested in a larger population and compared with the standard practice.

4.3. Phase analysis of atrial arrhythmias

Phase maps and SPs are commonly used to identify reentrant patterns in the atrial wall in animal models or in inverse–computed solutions [6,28,29] since they allow summarizing the propagation pattern without the need for activation detections which are highly sensitive to noise. We have shown that they can also be used for characterizing spatial reentrant patterns in the torso surface of atrial fibrillation patients [10]. Here, we further explore the ability of phase maps to represent rotational patterns in the torso surface which may not be univocally linked to functional rotors but to rotations around anatomical obstacles as well. Although surface representation of both entities is similar, they can be easily differentiated because of the differences in the rotation frequency, below 5 Hz in AFL, and in their spatio–temporal stability, since centers of rotational activity in atrial fibrillation tend to drift. In this proof-of-concept study, it is clearly depicted how a rotational behavior around a single obstacle may result in a figure-of-eight representation related with the reentrant activity rotational axis.

4.4. Limitations and future work

In this work we have shown that the location of phase singularities in surface maps is different for typical and atypical AFL patients. However, because of the limited number of patients included in our study we could not quantify its diagnostic value. A prospective study in a larger database should be performed to determine the sensitivity and specificity of the proposed criterion for the diagnosis of cavotricuspidius dependent AFL circuits and its potential in the identification of different atypical AFL reentrant circuits.

Since the identification of the reentrant circuit was not accomplished in the electrophysiological laboratory in non-cavotricuspidius dependent patients, we cannot relate the location of surface PSs and the anatomical location of the reentrant circuit in this group of patients. In addition, the identification of AFL typical flutter patients was based in the arrhythmia termination after cavotricuspid isthmus ablation. To explore the ability of surface phase maps to identify AFL reentrant circuits, further analyses should be performed with larger study groups including invasive electrophysiological studies that characterize clearly the reentrant circuits.

Finally, the proposed surface phase map analysis requires at least two atrial waves free from ventricular content, to avoid detection of SPs corresponding to ventricular activity. In this work we have performed carotid sinus massage to reduce the heart rate, which should not be performed in patients with carotid sinus hypersensitivity.

With respect to computational modeling, we simulated representative behaviors for typical flutter and atypical reentrant patterns. However, the variability of reentry circuits, conduction velocities etc. is very high in patients. Besides, the method of resolution of the forward problem considered the torso homogeneous medium, small deviations may be expected in SPs caused by refraction in different tissues. Despite these limitations, robustness of the method against noise and torso volume have been demonstrated, and therefore, the main conclusions presented here should hold.

5. Conclusion

Using noninvasive surface phase mapping during atrial macro-reentries, different rotational propagation patterns that are dependent on the structure that maintains the arrhythmia can be observed. This mapping procedure may help in the stratification of AFL patients and in the determination of the reentrant circuits sustaining the arrhythmia.

Conflicts of interest

Dr Atienza served on the advisory board of Medtronic and Livanova. None of the companies disclosed here financed the research described in this article. The other authors report no conflicts.

Acknowledgements

Supported in part by: Instituto de Salud Carlos III FEDER (Fondo Europeo de Desarrollo Regional; IJCI- 2014-22178, DTS16/00160; PI16/01123; PI17/01059; PI17/01106), Spanish Ministry of Education

and Generalitat Valenciana Grants APOSTD/2017 and APOSTD/2018.

The authors would like to thank Victoria Donis, Maria Mozo and Natividad Mihi for their help in data collection.

Appendix A. Supplementary data

Supplementary data to this article can be found online at https://doi.org/10.1016/j.compbiomed.2018.11.020.

References

[1] F. Garcia-Cosio, A. Pastor Fuentes, A. Nunez Angulo, Clinical approach to atrial tachycardia and atrial flutter from an understanding of the mechanisms. Electrophysiology based on anatomy, Rev. Esp. Cardiol. 65 (2012) 363–375, https://doi.org/10.1016/j.rec.2011.11.013.

[2] N. Saoudi, A classification of atrial flutter and regular atrial tachycardia according to electrophysiological mechanisms and anatomical bases. A Statement from a Joint Expert Group from the Working Group of Arrhythmias of the European Society of Cardiology and the, Eur. Heart J. 22 (2001) 1162–1182, https://doi.org/10.1053/euhj.2001.2658.

[3] F. Morady, Drug therapy - radio-frequency ablation as treatment for cardiac arrhythmias, N. Engl. J. Med. 340 (1999) 534–544.

[4] A. Da Costa, J. Thevenin, F. Roche, et al., Results from the Loire-Ardeche-Drome-Isere-Puy-de-Dome (LADIP) Trial on Atrial Flutter, a multicentric prospective randomized study comparing amiodarone and radiofrequency ablation after the first episode of symptomatic atrial flutter, Circulation 114 (2006) 1676–1681, https://doi.org/10.1161/CIRCULATIONAHA.106.638395.

[5] M. Yokokawa, R. Latchamsetty, H. Ghanbari, et al., A. Chugh, Characteristics of atrial tachycardia due to small vs large reentrant circuits after ablation of persistent atrial fibrillation, Heart Rhythm 4 (2013) 469–476.

[6] S. Zlochiver, M. Yamazaki, J. Kalifa, et al., Rotor meandering contributes to irregularity in electrograms during atrial fibrillation, Heart Rhythm 5 (2008) 846–854, https://doi.org/10.1016/j.hrthm.2008.03.01.

[7] M. Rodrigo, A.M. Climent, A. Liberos, et al., Highest dominant frequency and rotor positions are robust markers of driver location during noninvasive mapping of atrial fibrillation: a computational study, Heart Rhythm 14 (2017) 1224–1233, https://doi.org/10.1016/j.hrthm.2017.04.017.

[8] M. Rodrigo, A.M. Climent, A. Liberos, et al., Technical considerations on phase mapping for identification of atrial reentrant activity in direct-And inverse-computed electrograms, Circ. Arrhythmia Electrophysiol. 10 (2017), https://doi.org/10.1161/CIRCEP.117.005008.

[9] A.M. Climent, M.S. Guillem, L. Fuentes, et al., The role of atrial tissue remodeling on rotor dynamics: an in-vitro study, Am. J. Physiol. Heart Circ. Physiol. (2015), https://doi.org/10.1152/ajpheart.00055.2015 ajpheart.00055.2015.

[10] M. Rodrigo, M.S. Guillem, A.M. Climent, et al., Body surface localization of left and right atrial high frequency rotors in atrial fibrillation patients: a clinical-computational study, Heart Rhythm 11 (2014) 1584–1591, https://doi.org/10.1016/j.hrthm.2014.05.013.

[11] M.S. Guillem, A.M. Climent, J. Millet, et al., Noninvasive localization of maximal frequency sites of atrial fibrillation by body surface potential mapping, Circ. Arrhythmia Electrophysiol. 6 (2013) 294–301, https://doi.org/10.1161/CIRCEP.112.000167.

[12] M.S. Guillem, A. Quesada, V. Donis, et al., Surface wavefront propagation maps: non-invasive characterization of atrial flutter circuit, Int. J. Bioelectromagn. 11 (2009) 22–26.

[13] M.W. Krueger, V. Schmidt, C. Tobon, et al., Modeling atrial fiber orientation in patient-specific geometries: a semi-automatic rule-based approach, Lect. Notes Comput. Sci. 6666 (2011) 223–232.

[14] J.T. Koivumaki, G. Seemann, M.M. Maleckar, P. Tavi, In Silico screening of the key cellular remodeling targets in chronic atrial fibrillation, PLoS Comput. Biol. 10 (2014) e1003620, , https://doi.org/10.1371/journal.pcbi.1003620 e1003620.

[15] O. Doessel, M.W. Krueger, F.M. Weber, M. Wilhelms, G. Seemann, Computational modeling of the human atrial anatomy and electrophysiology, Med. Biol. Eng. Comput. 50 (2012), https://doi.org/10.1007/s11517-012-0924-6.

[16] A. SippensGroenewegen, M.D. Lesh, F.X. Roithinger, et al., Body surface mapping of counterclockwise and clockwise typical atrial flutter: a comparative analysis with endocardial activation sequence mapping, J. Am. Coll. Cardiol. 35 (2000) 1276–1287, https://doi.org/10.1016/S0735-1097(00)00549-0.

[17] K. Sasaki, S. Sasaki, M. Kimura, et al., Revisit of typical counterclockwise atrial flutter wave in the ECG: electroanatomic studies on the determinants of the morphology, Pace-Pacing Clin. Electrophysiol. 36 (2013) 978–987, https://doi.org/10.1111/pace.12129 ER.

[18] V.M. Garcia-Molla, A. Liberos, A. Vidal, et al., Adaptive step ODE algorithms for the 3D simulation of electric heart activity with graphics processing units, Comput. Biol. Med. 44 (2014) 15–26, https://doi.org/10.1016/j.compbiomed.2013.10.023.

[19] B.M. Horacek, J.C. Clements, The inverse problem of electrocardiography: a solution in terms of single- and double-layer sources on the epicardial surface, Math. Biosci. 144 (1997) 119–154.

[20] J. Pedrón-Torrecilla, M. Rodrigo, A.M. Climent, et al., Noninvasive estimation of epicardial dominant high-frequency regions during atrial fibrillation, J. Cardiovasc. Electrophysiol. 27 (2016) 435–442, https://doi.org/10.1111/jce.12931.

[21] R.S. Macleod, C.R. Johnson, P.R. Ershler, Construction of an Inhomogeneous Model of the Human Torso for Use in Computational Electrocardiography, I E E E, New York; New York, 1991, https://doi.org/10.1109/IEMBS.1991.684145.

[22] C. Medi, J.M. Kalman, Prediction of the atrial flutter circuit location from the surface electrocardiogram, Europace 10 (2008) 786–796, https://doi.org/10.1093/europace/eun106.

[23] D.E. Krummen, G.K. Feld, S.M. Narayan, Diagnostic accuracy of irregularly irregular RR intervals in separating atrial fibrillation from atrial flutter, Am. J. Cardiol. 98 (2006) 209–214, https://doi.org/10.1016/j.amjcard.2006.01.088.

[24] J.G. Akar, M.O. Al-Chekakie, A. Hai, et al., Surface electrocardiographic patterns and electrophysiologic characteristics of atrial flutter following modified radiofrequency MAZE procedures, J. Cardiovasc. Electrophysiol. 18 (2007) 349–355, https://doi.org/10.1111/j.1540-8167.2007.00761.x.

[25] D.E. Krummen, M. Patel, H. Nguyen, et al., Accurate ECG diagnosis of atrial tachyarrhythmias using quantitative analysis: a prospective diagnostic and cost-effectiveness study, J. Cardiovasc. Electrophysiol. 21 (2010) 1251–1259, https://doi.org/10.1111/j.1540-8167.2010.01809.x.

[26] J.G. Kall, D.S. Rubenstein, D.E. Kopp, et al., Atypical atrial flutter originating in the right atrial free wall, Circulation 101 (2000) 270–279.

[27] A.M. Kahn, D.E. Krummen, G.K. Feld, S.M. Narayan, Localizing circuits of atrial macroreentry using electrocardiographic planes of coherent atrial activation, Heart Rhythm 4 (2007) 445–451, https://doi.org/10.1016/j.hrthm.2006.12.042.

[28] M. Yamazaki, S. Mironov, C. Taravant, et al., Heterogeneous atrial wall thickness and stretch promote scroll waves anchoring during atrial fibrillation, Cardiovasc. Res. 94 (2012) 48–57, https://doi.org/10.1093/cvr/cvr357.

[29] M. Haissaguerre, M. Hocini, A.J. Shah, et al., Noninvasive panoramic mapping of human atrial fibrillation mechanisms: a feasibility report, J. Cardiovasc. Electrophysiol. 24 (2013) 711–717, https://doi.org/10.1111/jce.12075.